Optical and Quantum Electronics (2024) 56:901
https://doi.org/10.1007/s11082-024-06719-7

Impact of laser parameters on synthesis zinc oxide nanoparticles and evaluation of its antibacterial activity

Sara Fadhil Abbas[1] · Adawiya J. Haider[2] · Sharafaldin Al-Musawi[3] · Murtadha Kadhim Selman[4]

Received: 27 December 2023 / Accepted: 19 February 2024 / Published online: 10 April 2024

Abstract

Antibiotic resistant pathogen is one of the most urgent issues facing global health care. Zinc oxide nanoparticles (ZnO NPs) have demonstrated a strong antibacterial capacity against both gram-positive and gram-negative bacteria, according to a number of studies. In the present study, ZnO NPs were synthesized using laser ablation in water technique by various laser energies and wavelengths. The optical absorption study proves the high peak absorption and the blue shift at 1000 mJ laser energy and 1064 nm wavelength. UV visible spectroscopy shows an absorption peak seen at (255–342) nm and the estimated optical band gap was 3.8 eV. Fourier transform infrared spectroscopy confirms the appearance of stretching mode Zn–O bond at 667 cm^{-1}. The notice Raman peaks at 437 and 380 cm^{-1} were assign to the E2 (high) and A1(TO) modes respectively. The broad band at 330 cm^{-1} is due to second order Raman scattering. X-ray diffraction shows a hexagonal wurtzite phase of ZnO at $2\theta \approx$ (32.5°, 33.9°, 37.1°, 57.24°, and 63.6°) correspond to the diffraction planes of (100), (002), (101), and (110), (103), respectively. Chemical composition using Energy Dispersive X-Ray analysis ensured the high purity sharp peaks for Zn and O. High-Resolution Transmission Electron Microscope HR-TEM showed the creation of hexagon-shaped ZnO nanoparticles with average particle diameter of the produced ZnO nanoparticles was found to be 35 ± 5.1 nm. Dynamic light scattering shows particle size of 35 nm and zeta potential of -37 mV which means high dispersity. Bacterial sensitivity test shows interesting antibacterial activity in concentration dependent manner and there is a remarkable effectiveness of ZnO NPs against negative gram *Escherichia coli* than positive gram strain *Staphylococcus aureus*.

Keywords Antibacterial activity · Antibiotic · *Escherichia coli* · Laser ablation · *Staphylococcus aureus*, · Zinc oxide

✉ Adawiya J. Haider
adawiya.j.haider@uotechnology.edu.iq

[1] Department of Laser and Optoelectronics Engineering, College of Engineering, Al-Nahrain University, Jadriya, Baghdad, Iraq

[2] Applied Sciences Department/Laser Science and Technology Branch, University of Technology, Baghdad, Iraq

[3] College of Food Sciences, Al-Qasim Green University, Al-Qasim, Babylon Province, Iraq

[4] Ministry of Education - Babylon Education Directorate, Hillah, Babylon Province, Iraq

1 Introduction

Nanotechnology is the field of science takes care of studying the materials in size ranging 1–100 nm (Anu et al. 2020). There are several methods for synthesizing the nanoparticles lies in this range (Govindasamy et al. 2023a). The manufactured particles have different morphologies, such as nanospheres, nanorods, nanoribbons, nanobelts, and nanoplatelets (Thakur and Thakur 2023). Because of their size, shape, and large surface area, the NPs have special chemical and physical characteristics (Thakur and Thakur 2023; Govindasamy et al. 2023b; Balkrishna et al. 2021). Nanotechnology can be used for a variety of novel applications, such as advanced medical procedures, food processing, innovative fabric compounds, and agricultural productivity (Sahoo 2010; Pal et al. 2007; Ashe 2011; Batros et al. 2023). Their unique characteristic makes them potentially useful in a variety of sectors, including biosensors, nano-medicine, and bio-nanotechnology (Sirelkhatim et al. 2015; Kumar et al. 2023a).

It has been discovered that metals oxide nanoparticles have interesting antibacterial action (Sukhdev, et al. 2020; Basosila, et al. 2023; Kumar et al. 2023b). Zinc oxide NPs one of the most significant functional nanomaterial have a broad band gap energy (3.37 eV) and a substantial excitation binding energy (60 meV) (Tanna et al. 2015; Thakur et al. 2021). ZnO nanostructures in a variety of forms hold great potential for use in gas sensors, electrochemical sensors, light emitters, paints, personal hygiene products, catalysts, paints, display windows, and solar cell windows (Atrazina et al. 2011; Abbas et al. 2023). ZnO NPs can be utilized as an antibacterial agent since it possesses a number of qualities, such as strong antimicrobial activity, excellent thermal stability, and exceptional biocompatibility(Abebe et al. 2020). Different ZnO nanostructure morphologies show antibacterial activity against a variety of bacterial species that have been studied by many researchers (Zhu et al. 2016; Hosseini VeleshKolaei et al. 2023). Antibacterial activity can be defining as the process that stops or restricts the growth of bacteria. It can also be explained as a consequence of the surface area that is in touch with the microbes. When an antibacterial substance stops bacteria from growing or kills them, it is referred to as bacteriostatic. Several studies suggest that zinc oxide (ZnO) is a highly effective antibacterial agent against both gram positive (*Escherichia coli)* and gram negative (*Staphylococcus aureus*) bacteria (He et al. 2002; George et al. 2010; Yudasari et al. 2019).

ZnO NPs produced using different methods such as chemical, physical, and biological techniques. These methods include sol–gel, chemical process, thermal plasma, hydrothermal techniques, green synthesis, and laser ablation etc. (Jurablu et al. 2015; Madathil et al. 2007; Ko et al. 2006; Thakur and Kumar 2020; Haider et al. 2018).

Pulsed laser ablation in water (PLAW) approach may create high-purity nanomaterials in an easy and affordable preparation procedure without the need of a hazardous chemical mixture (Khashan 2016; Abdulwahid et al. 2023a). It is a physical top-down production technique based on the idea of splitting metal ion bulk precursors into the atoms of metal (Haider, et al. 2023; Ahmed et al. 2023). Researchers are interested in the PLAW because it is a good and modern way to create different kinds of nanomaterial. The success of the pulsed laser approach in creating various sized and shaped NPs that are utilized in several applications highlights its significance in a liquid environment (Abdulwahid et al. 2023b; Haider et al. 2021a).

Most notably, it has been shown that several parameters, including the wavelength of the laser, the fluence, laser pulse duration, solution pH, surfactant addition, and solution

temperature, may all be used to influence the size of synthesized material (Ishikawa et al. 2006; Solati et al. 2013; Drmosh et al. 2010).

In the presented study, the optimum condition of manufacturing ZnO NPs and its antibacterial activity against the both gram strains bacteria (positive and negative). the synthesizing of ZnO NPs by laser ablation method was environment friendly and a suitable method. In the subsequent sections, we have discussed extensively the physical properties of ZnO NPs in terms of morphology, optical properties, chemical composition, crystallinity, dispersity, and bonding energy. Then tested the antibacterial activity and the minimum inhibitory concentration (MIC) of different zinc oxide concentration comparing with silver nitride as a control agent.

2 Experimental work

2.1 Materials and methods

In the present study zinc oxide NPs produced using laser ablation in liquid method. A high purity zinc sheet (99.999%, BDH chemical Ltd pool, England) cutting to a small target ($1\times1\times0.1$) cm and cleaned with ethanol, acetone and distilled water to leftover any unwanted organic impurities. XRD pattern of the pure zinc sheet employed in this work showed in Fig. 1.

The target placed in a small glass vessel contain 5ml of distilled deionized water (DW) at room temperature. Applying Nd:YAG laser Q-switched (Huafei Tongda Technology-DIAMOND-288 pattern EPLS) of a specific characterization: (532 nm, 1064 nm) wavelength, (600, 800, 1000) mJ laser energy, 25 min exposure time, and 10 ns pulse width. The laser beam was focused on the target using convex lens of 10 cm focal length. As a first insight of producing NPs the water color varied and tend to turbid brown. The PLAW process represent in Fig. 2.

Previous research has classified the reactions involved in the production of ZnO nanostructures by PLAW into two categories: chemical and physical responses (Abbas et al.

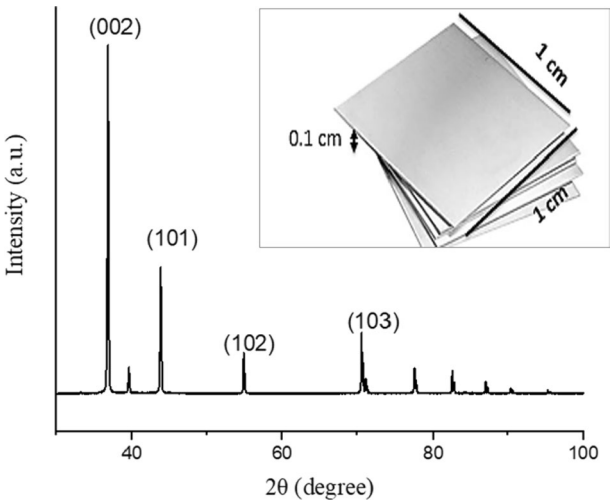

Fig. 1 XRD of the zinc sheet used in our work (inset:target dimension)

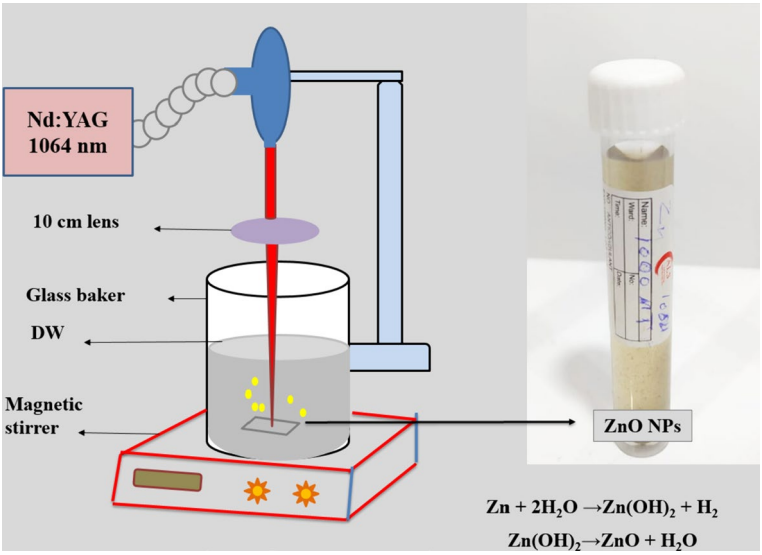

Fig. 2 pulsed laser ablation in water (PLAW) process

2023; Al-Kinani et al. 2021). The temperature of the illumination spot quickly rises when the laser beam concentrates on the solid target material's surface in the liquid media, evaporating the target material (Yousif et al. 2012; Haider et al. 2022). A dense zinc plasma zone forms on the liquid–solid boundary when a laser beam is ablated onto the zinc metal surface. In this experiment, the liquid medium is distilled water. This adds extra pressure to the plasma and limits its expansion, making it denser than the plasma created in the absence of liquid environment (Khashan and Abbas 2019). Zinc clusters are created when the plasma extinguishes after expanding adiabatically and rapidly. A cavitation bubble is created when the plasma vanishes and grows gradually till it collapses at its largest size (Khashan and Abbas 2016; Haider et al. 2021b). It is thought that the collapse of the cavitation bubble, which releases high pressure and temperature into the surrounding environment, aids in the creation of ZnO NPs. In the meantime, zinc hydroxide, $Zn(OH)_2$ will further break down to make ZnO are formed when the zinc clusters generated by plasma react with the surrounding water medium (Al-Obaidy et al. 2023).

2.2 Characterization of ZnO

The ZnO NPs were identified by using a twin beam UV–VIS spectrophotometer (Shimadzu UV-1800), the optical absorption of colloidal NPs was determined between 200 and 800 nm. Using Shimadzu 8000 Series Fourier transform infrared (FTIR) spectroscopy, the bond vibrations of NPs in the 400–4000 cm^{-1} range were detected. Raman scattering measurements of ZnO NPs, were performed in the backscattering geometry by Raman microscope (LabRAM Aramis, Horiba Jobin Yvon S.A.S, Lille, France), equipped with a laser source operating at 532 nm at room temperature, in the air. Using CuK at 1.5406 Å wavelengths, X-ray diffraction (XRD) studies were carried out at 40 kV and 30 mA (AERIS PAN analytical, Japan). Using increments of 0.05°/s, the samples were examined

at intervals of 2θ between 20 and 80°. High-Resolution Transmission Electron Microscope (JEM-2000 EXII, JEOL, Tokyo, Japan) at 120 kV are used for study the morphology of the nanostructures. For HR-TEM, the sample solution placed on a 200 mesh formvar carbon-coated copper grid (TABB Laboratories Equipment). The sample's chemical composition disperses X-ray energy (Axia Chemi scanning electron microscope). Zeta potential and particle diameter are confirmed by dynamic light scattering (DLS) (Malvern Zetasizer ZS, Malvern, UK).

2.3 Antibacterial study

A variety of techniques have been used to evaluate and research antibacterial activity in vitro. Agar dilution, the microtiter plate-based technique, disk diffusion, and broth dilution are some of these techniques (Premanathan et al. 2011). Using the experiment of agar disc diffusion, the antibacterial activity of five different doses of ZnO NPs were observed. In order to make sure there is no contamination, the agar plates used for the antibacterial test were incubated for the entire night. After being removed from the agar plates, the isolated bacteria were put into 100 ml of nutritional broth. The Orbital Shaker Incubator was used to incubate the bacterial suspension overnight at 37 °C and 100 rpm. With a sterile glass spreader that was 90 degrees bent, 100 µl of bacterial suspension was applied to the nutritional agar surface. For 48 h, the plates containing ZnO NPs and bacteria were incubated at 37 °C. Using a meter ruler, the diameter of each inhibition zone was measured after the inhibition zones of each sample were examined. Antibacterial examination was performed on two bacterial strains positive gram (*Staphylococcus aureus*, ATCC 25922, NCTC 8532 [IAM 12544, R. Hugh 2605]) and negative gram (*Escherichia coli*, ATCC 25922, FDA strain Seattle 1946 [DSM 1103, NCIB 12210]).

2.4 Statistical analysis

The mean ± standard division (SD) was used for the statistical analysis of our results. SPSS version 27 was used to evaluate statistical significance. Results $p < 0.05$ and $p < 0.01$ are defined as the criteria for statistical significance.

3 Results and discussions

3.1 Choose optimized parameter

The use of UV–vis spectrum can be considered as a first indication of NPs properties. In this study two parameter of laser altered: laser energy (600, 800, and 1000) mJ and wavelength (1064 and 532) nm. The generation of ZnO NPs via PLAW is confirmed by the strong absorption peak seen ranging from (255–342) nm. It is clear that a sizable abrupt absorption of ZnO signifies that the dispersion of NPs is mono-dispersed. The characteristics absorption peak of hexagonal wartizite ZnO was less than 400 nm (Umar et al. 2022). Because of ZnO's direct bandgap, this distinctive peak of absorption is a consequence of various factors including doping, surface imperfections, crystallinity, and particle size. The absorption peak shifts to the blue as a result of increased quantum confinement effects caused by ZnO nanoparticle size reduction. These results make a good agreement with the previous reported (Talam et al. 2012; Goh et al. 2014). The excitonic absorption of the

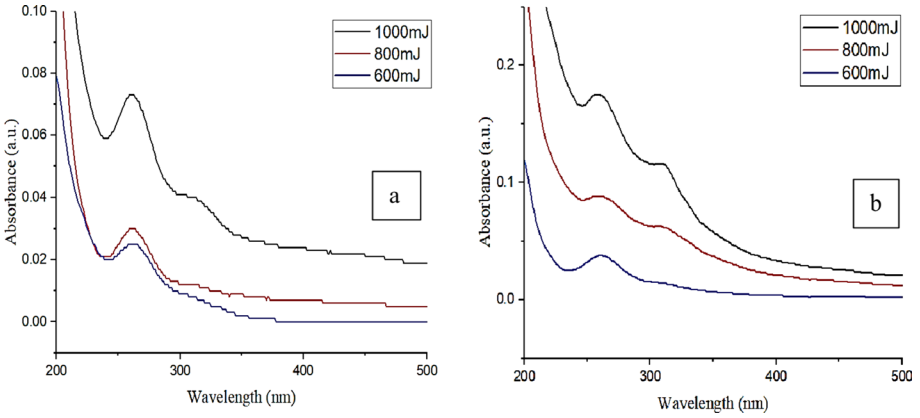

Fig. 3 UV–vis absorbance of different laser energy (1000, 800, and 600) mJ (**a** 532 nm, **b** 1064 nm)

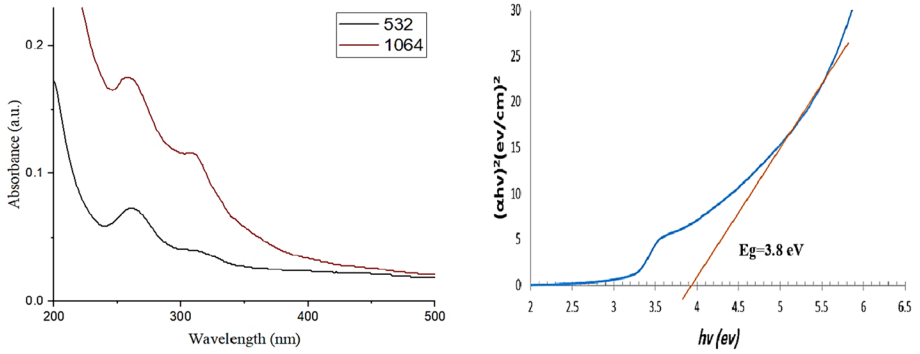

Fig. 4 **a** UV–vis absorbance of different laser wavelength at 1000 mJ laser energy. **b** Band gap of the optimum ZnO NPs

produced ZnO NPs showed a notable blue-shift when compared to the bulk ZnO (373 nm) (Xin-Hua et al. 2006; Debanath and Karmakar 2013).

Regarding the laser pulse energy, earlier studies have demonstrated that an increase in laser pulse energy resulted in an increase in the number of particles ablated (Solati et al. 2014). This explained in high productivity and raise in the absorbance peak. A substance's absorbance is correlated with its concentration. This term explains as the amount of light which is absorbed depends on the number of molecules that the light interacts with. This concept is evident from our findings which is preview in Fig. 3a and b. Comparing the value of absorbance as a function to the laser energy, it is found maximum absorbance in the sample prepared at 1000 mJ. This behavior was apparently for both wavelengths used.

The effect of wavelength can be explained as a function of photon energy. The number of particles reduces with increasing photon energy when the pulse energy stays constant. This could be the reason why photon energy is less important to the ablation rate than photon number. A lower absorbance amount clearly demonstrates that there are less particles in samples created by a 532 nm laser pulse.

Figure 4a comparing the effect of changing wavelengths (1064 and 532) nm at a constant laser energy 1000 mJ. The peak absorbance at 1064 nm was little shift towards

blue region. The excitation absorption's blue-shift amply demonstrates NPs' quantum confinement feature. The absorption edge shifted to a lower wavelength when the particle size shrank in the quantum confinement range due to a rise in the particle's band gap.

From the results shown above, it can clearly see that using the highest laser power, which is 1000 mJ and the wavelength 1064 nm, gave the best results. These best results will apply for all the next analysis.

The band gap estimated using Tauc plot study for the sample of the optimum condition was presented in Fig. 4b. The optical band gap was 3.8 eV this was compatible with earlier findings(Debanath and Karmakar 2013; Almaary et al. 2023).

3.2 FTIR analysis

FTIR spectroscopy concedered as a flexible method for examining chemical interactions in a range of substances, including liquids, solids, and gases. Researchers can aquire important information about molecule structure, bonding, conformational dynamics, and intermolecular interactions within the sample by examining the spectrum patterns and changes shown in FTIR data. Figure 5 illustrates the ZnO NPs' prepared using the optimum ablation results which was identified via FTIR spectroscopy. O–H stretching vibrations is the fundamental mode vibration caused considerable absorption band at 3435 cm^{-1}. The peak observed at 2075 cm^{-1} referred to the presence of C=O stretching mode due to the existence of carbon in the environment. There is another peak located at 1634 cm^{-1} correspond to bending stretching mode of O–H. The fingerprint area, or below 1000 cm^{-1}, is where metal oxides typically display absorption bands caused by interatomic vibrations (Khan, et al. 2016). Peak at 667 cm^{-1} indicate that ZnO NPs are in a stretching vibration mode which is in good agreement with (Sagar Raut 2015; El-Gammal 2016).

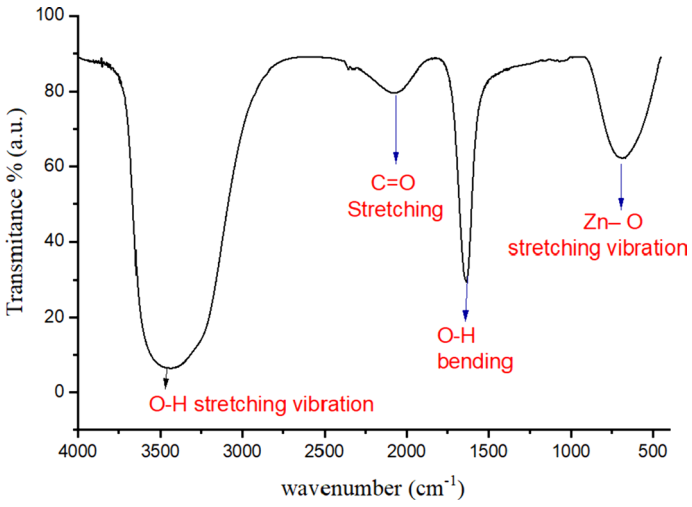

Fig. 5 FTIR spectra of ZnO NPs prepared by PLAW

3.3 Raman shift

The Raman signals exhibit high sensitivity to both crystal defects and crystal structure. ZnO has a wurtzite (hexagonal) crystal structure, which is a related to the C_{6v}^4 space group. Each primitive cell in this group has two formula units, and all of the atoms occupy the C_{3v} sites (Khan 2010). The vibration phonons are usually divided into eight sets: the polar A1 and E1 mode divides into longitudinal optical (A1L and E1L) and transverse optical (A1T and E1T) phonons, and the E2 mode consists of two Raman-active low-frequency and high-frequency phonon modes (E2L and E2H) (Junlabhut et al. 2014). The irreducible representations $\Gamma_{opt} = A1 + E1 + 2E2 + 2B1$ can be used to categorize the zone-center optical phonons. The A1 and E1 modes are polar and both Raman and infrared active, while the B1 modes are silent. The E2 modes are nonpolar and only Raman active (Cuscó et al. 2007).

Figure 6 shows Raman scattering spectra at room temperature. The most prominent sharp peak, denoted as E2 (high), was detected at 437 cm^{-1}. This peak is recognized as the Raman-active optical phonon mode and is typical of the wurtzite hexagonal phase ZnO. The Raman processes of second ordered are responsible for the peak observed at 330 cm^{-1} (Zhou et al. 2013).The peak appeared at 380 cm^{-1} belongs to A1(TO). The peak at 331 cm^{-1} referred to $E_2^{high} - E_2^{low}$ (Šćepanović et al. 2010).

3.4 XRD analysis

The produced ZnO NPs' XRD pattern was obtained as illustrated in Fig. 7. As mention above, the sample prepared using (1000 mJ, 1064 nm). According to the electron diffraction data, the XRD pattern shows that the hexagonal wurtzite phase of ZnO has formed. The hexagonal wurtzite phase is significant in the field of antibacterial activity because it has a high surface area-to-volume ratio that facilitates better contact with bacterial cells. Also, wurtzite phase can improve ZnO NPs' ability to enter bacterial cells and hence increase their antibacterial action. The XRD pattern's peak broadening amply demonstrates the presence of tiny nanocrystals in the samples. No indications of impurities or bulk residual materials are present. The produced particles' good crystallinity is indicated by the strong diffraction peaks. Zinc atoms occupy half of

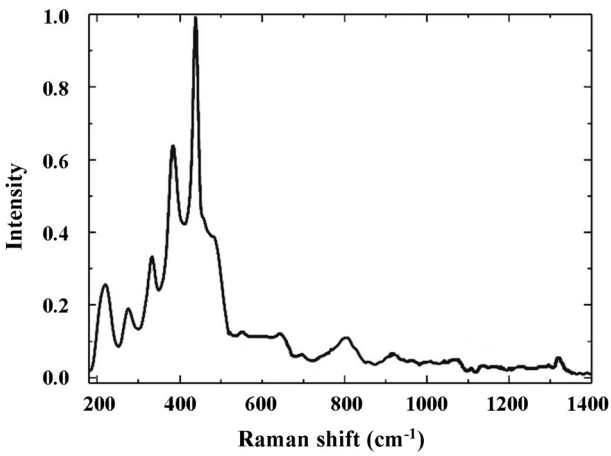

Fig. 6 Room temperature Raman spectra of ZnO NPs

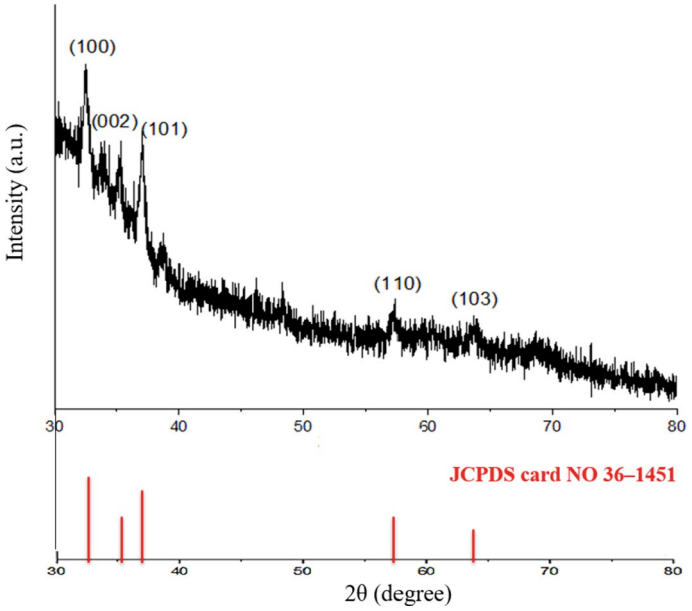

Fig. 7 XRD patterns of ZnO NPs with standard (JCPDS card NO 36–1451)

the tetrahedral sites in ZnO crystallizes in the wurtzite structure, where oxygen atoms are organized in a hexagonal close-packed form. A number of peaks at 2θ ≈ (32.5°, 33.9°, 37.1°, 57.24°, and 63.6°) are visible in the figure, which correspond to the diffraction planes of (100), (002), (101), and (110), (103), respectively, representing zinc oxide hexagonal nanostructure (JCPD 00–036-1451). Table 1 shows the important XRD parameter. Using the data of XRD analysis, the estimated ZnO NP size was determined via the use of Debye–Scherrer's (Khashan and Abbas 2019; Haider et al. 2019) formula, which yields the following equation:

$$D = \frac{0.9\lambda}{\beta \mathrm{Cos}\theta} \tag{1}$$

where β is the full width half maximum (FWHM) and λ is the X-ray wavelength, which is equivalent to 1.5406 Å. Consequently, it is possible to determine that the ZnO NPs' typical crystallographic size is 42nm. Wang et al. and Dash et al. have both produced findings that are comparable (Dash et al. 2019; Wang et al. 2015).

Table 1 summarized XRD analysis details of ZnO NPs

Pos. [°2θ]	Crystallite size [Å]	d-spacing [Å]	Orientation
32.5	451	2.7527	(100)
33.9	182	2.63945	(002)
37.1	456	2.4218	(101)
57.24	198	1.60813	(110)
63.6	204	1.46212	(103)

3.5 Morphological analysis

More information of studying ZnO NPs morphology obtained by TEM analysis presented in Fig. 8a. TEM micrographs showed the creation of hexagon-shaped ZnO nanoparticles, with sizes ranging from 10 to 80 nm. This confirms the results obtained from the XRD analysis. Our findings match with those of Flemban (2023), who verified the environmentally friendly synthesis of ZnO nanoparticles using laser ablation that had spherical and hexagonal shapes. The mean particle diameter of the produced ZnO nanoparticles was found to be 35 ± 5.1 nm, according to the particle size distribution (Fig. 9b).

The elemental composition of ZnO NPs generated by laser was investigated using EDX, as shown in Fig. 9a. ZnO NP production is indicated by the sharp peaks for Zn and O, which are shown to be 39.2% and 53.5%, respectively, in the EDX spectra. The presence of small peak of 7.3% of carbon can be attributed to the laboratory circumstances. The high purity of the prepared ZnO NPs as antibacterial agent is very important manner. confirming the high purity of ZnO NPs is crucial for maximizing their antibacterial effectiveness, biocompatibility, and accuracy in various applications, such as wound healing.

Figure 9b–d shows ZnO NPs film provided the elemental maps (C, Zn, and O) for EDX. The relative intensity scale (0–2) for C, Zn, and (0–3) in O case. the color presentation of each element in bright (element-rich) and black (element-deficient) states, respectively, are used to depict each map. Over the entire measured region, the elements exhibit a consistent and homogeneous distribution.

3.6 Dynamic light scattering

The average particle size of the produced ZnO NPs was established by dynamic light scattering (DLS) analysis. The particle size distribution vs. intensity presented in (Fig. 10a). DLS examination yielded an average particle size of 35 nm, which is agreement with the result presented from HR-TEM study revealed.

The polydispersity index (PDI) of the NPs can be found out via the DLS analysis. Important information about the homogeneity of particle sizes throughout the NP

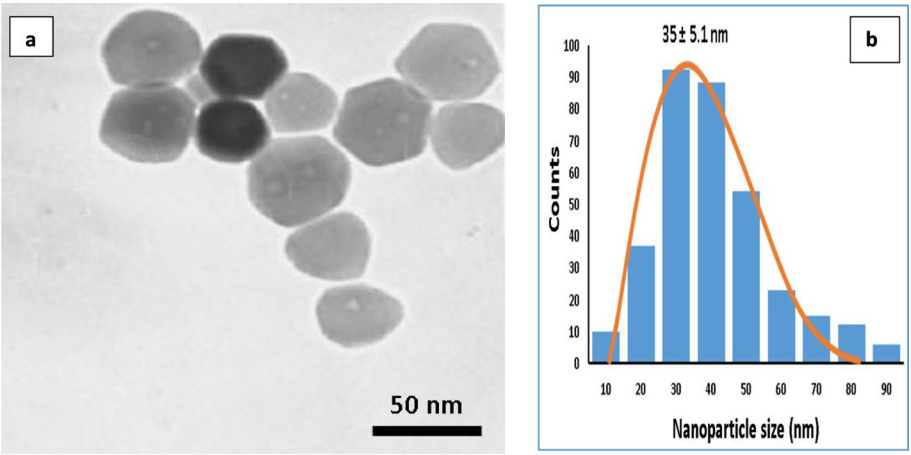

Fig. 8 **a** HR-TEM of ZnO NPs **b** histogram of ZnO NPs size distribution

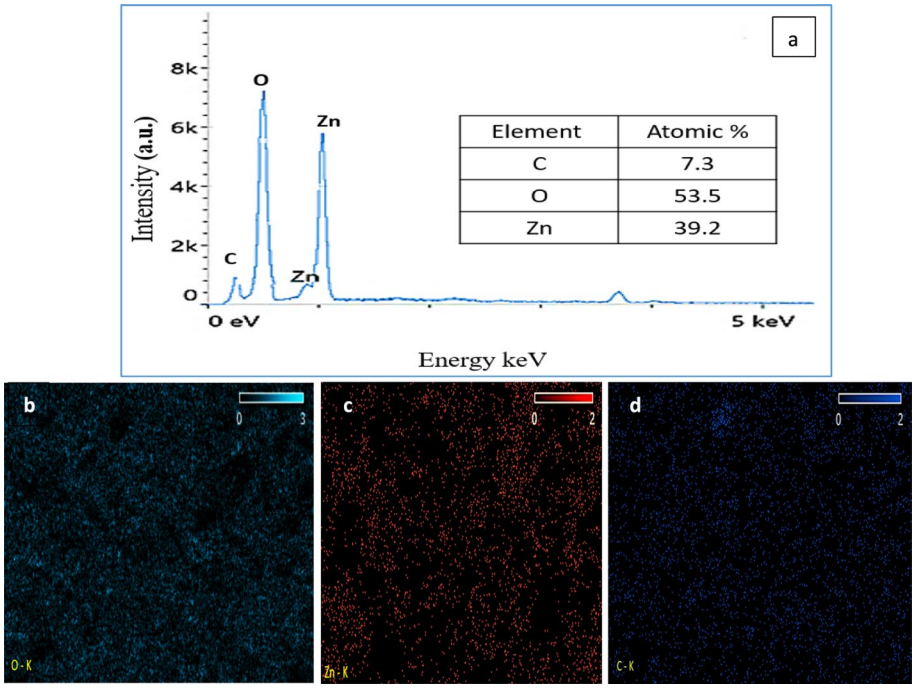

Fig. 9 **a** EDX analysis of ZnO NPs, **b**, **c** and **d** EDX analysis map of elements: O, Zn, and C, respectively

sample is provided by the PDI. The range of the PDI scale is 0 to 1. Suspension homogeneity is indicated by a PDI score of less than 0.4. Conversely, a PDI score above 1 indicates a high degree of heterogeneity in the suspension (Danaei et al. 2018). In this study the PDI estimated was 0.197 which represent the particle size distribution is very narrow.

The ZnO NPs' zeta potential measurement is shown in (Fig. 10b). One commonly utilized measure to predict the stability of colloidal suspension of produced ZnO NPs is the zeta potential. Since alterations to these characteristics have a substantial impact on a NPs's biological function, this analytical tool is dependable and easy to use for examining the electrostatic charge on the surfaces of NPs in a colloidal dispersion. It also offers insights into the stability and aggregation of NPs. It indicates the strength of the repulsion between particles in the dispersion medium that have similar charges. The negative charge of the NPs is related to their increased stability; that is, NPs with a higher negative charge (< -30) demonstrated stronger stability (Drmosh et al. 2010). Particle aggregate and poor dispersity may result from reduced repulsive interactions between particles, as indicated by a low or nearly zero zeta potential. Aggregation can cause irregular performance because it produces bigger particle clusters that settle out of solution more easily. The ZnO NPs' zeta potential values in the current investigation were (-37 mV). While the values of highly stable dispersions exceed approximately 30 mV, this outcome demonstrates the high stability of the NPs ablated by pulsed laser.

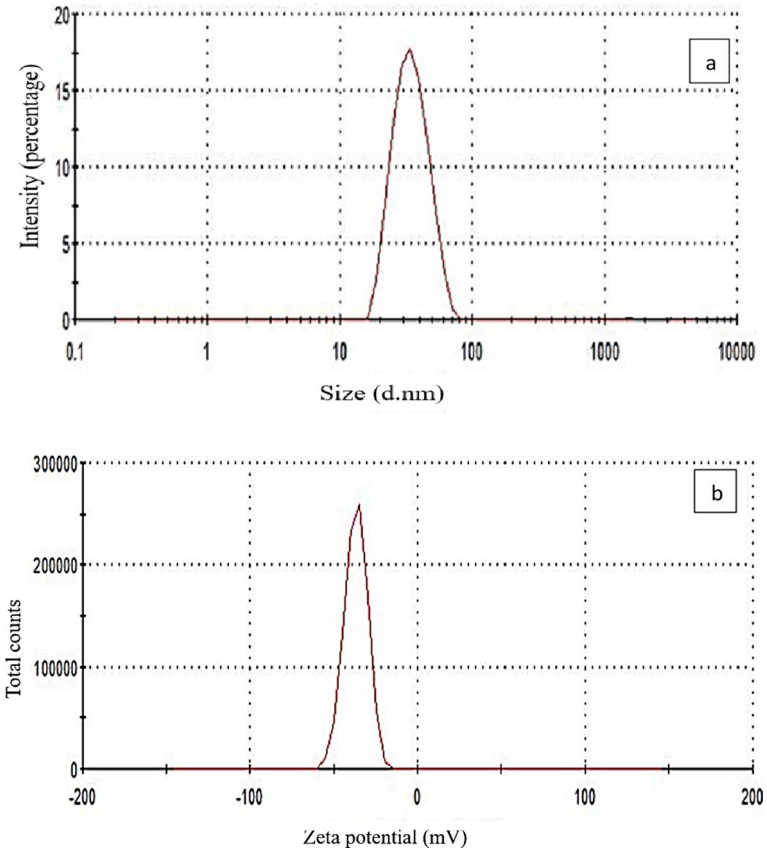

Fig. 10 illustrate ZnO NPs (**a** particle size distribution, **b** zeta potential)

3.7 Antibacterial activity

In the medical field, antibiotic resistant pathogen, are a serious problem. The complex mechanisms possessed by these antibiotic resistant pathogen strains enable them to resist the effects of antibiotics, thereby increasing the difficulty of treating and managing their infections (Salman et al. 2018). Scientists are continuously researching new active compounds like NPs, which have unique properties such their large surface area, compact size, and ability to penetrate bacteria, in order to improve their antimicrobial effect (Fouda et al. 2023). In comparison to its bulk material properties, ZnO demonstrates notable antibacterial capabilities at the nanoscale (Rashid et al. 2022). Because small particles have a larger surface area than larger ones, which can alter the biological functionality of some cells, particularly strains of bacteria (Ismail et al. 2018). The concentration of the NPs and the starting bacterial concentration have a considerable impact on the antibacterial activity of the particles (Abbas et al. 2023). Therefore, in this work, the concentration of the NPs is the primary determinant of their antibacterial activity. Because the NPs' vast surface area increases with decreasing particle size, their antibacterial activity increases as well, increasing their membrane permeability. It is thought that the process by which ZnO's

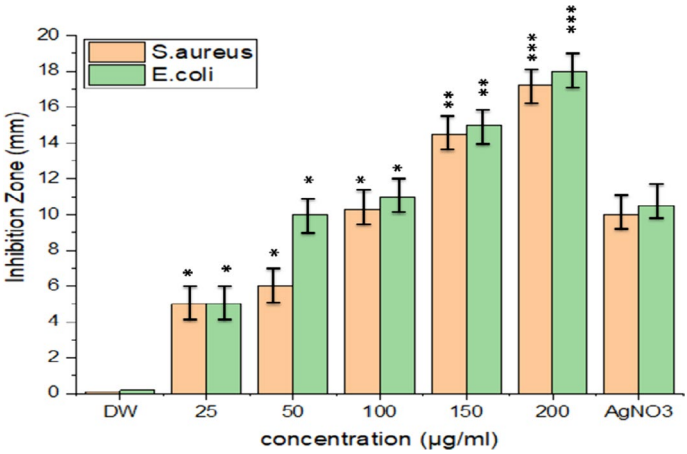

Fig. 11 Antibacterial activity of ZnO NPs against *E. coli* and *S. aureus*. (DW: distilled water, $AgNO_3$: control agent). Data are presented as (mean ± SD (*$p < 0.05$; **$p < 0.01$; ***$p < 0.001$); n = 3)

Table 2 Antibacterial activity of ZnO NPs

Bacterial strain	Inhibition zone (mm)							
	Concentration µg/ml	DW	25(MIC)	50	100	150	200	$AgNO_3$
Positive-gram *S. aureus*		0	5	6	10.25	14.5	17.2	10
Negative-gram *E. coli*		0.2	5	10	11	15	18	10.2

surface produces hydrogen peroxide, which stops bacterial growth, is what breaks down bacterial cells.

Here, ZnO NPs manufactured by employing the PLAW technique and choosing the optimum condition. In this work, the antibacterial activity of zinc oxide NPs against both strains gram-positive (*S. aureus*) and gram-negative (*E. coli*) bacteria is interesting. It was found that the level of inhibition of bacterial growth observed in this study varied and was concentration-dependent. The antibacterial activity of ZnO NPs against *S. aureus* and *E. coli* is displayed in Fig. 11. In this work various concentrations were employed (25, 50, 100, 150, and 200) µg/ml in antibacterial assay. The use of clean distilled water is represented by the first column (DW), and the usage of silver nitride ($AgNO_3$) is shown by the last (control agent). The effect of high concentration NPs exceeded the effect of the control agent $AgNO_3$. The values of the affectivity recorded in details at Table 2. There is a remarkable difference in the antibacterial activity of ZnO NPs against negative gram than positive gram strain. The results of this work in good agreement with previous study (Azam et al. 2012). The electrostatic interaction between the positive charge of NPs and the negative charge of bacterial cell surfaces is generally what drives NPs' antibacterial activity, and it is essential to NPs' ability to function as bactericidal agents (Maqbool, et al. 2016). The release of ROS onto the NPs' surface, which binds to the surface and damages the bacteria via electrostatic forces, could account for the proposed inhibitory mechanism. Furthermore, it was proposed that the mechanical contact between the bacteria and the

Table 3 Summarized previous publications on ZnO NPs as a detailed comparison study

Method [References]	Shape	Size nm	Concentration	Inhibition zone (mm)	
				E. coli	*S. aureus*
[The present study] laser ablation	Hexagonal	35 ± 5.1	200 µg/mL	18	17.2
Green synthesis (Ashwini et al. 2021)	Hexagonal	32	(250, 500, 1000) µg/ml	18	13
Chemical method (Bhosale et al. 2021)	Spherical	15–20	25 (mg/ ml)	19	20
Sol–gel (Azam et al. 2012)	Spherical	18	–	18	16
Sol–gel (Khan, et al. 2014)	Flower	23.7–88.8	0.50 (mg/ml)	21	20
Green synthesis (Ehsan and Sajjad 2017)	Hexagonal	66	20 µg/ml	–	17.4 (impregnated with antibiotics)
Solvothermal method (Zare et al. 2018)	Rod, flower	20–30	0.625 (mg/ml)	10	17
Chemical deposition(Shinde 2015)	Hexagonal and spherical	20–25	0, 20, 40, 60, 80 and 100 µg/ml	–	Zno nps retards the growth of the bacterial present in suspension
Laser ablation in solution (Yudasari et al. 2019)	Rod	20–100	0–750 µl	There are no survived bacteria found as used 20%, 25% and 30% zno-nps	–
Chemical method (Anwar et al. 2020)	Rod	20–30	250 µg/ml	5.33	–

ZnO surface, caused by free Zn^{+2}, largely led to an antibacterial effect (Cruz et al. 2020). Table 3 shows various shapes ZnO NPs produced using different methods from previous publications as a detailed comparison study.

4 Conclusion

The synthesize of ZnO NPs with varying laser ablation energies and laser wavelengths was investigated. The prepared ZnO NPs' size and concentration are influenced by the energy of the PLAW. It can be concluded at higher laser energies and wavelengths; the concentration rises and the particle size decreases. The optimum laser parameter was 1064 nm wave length at 1000 mJ laser energy. The manufactured ZnO NPs was wurtzite, hexagonal shape, high disparsity − 37mV, narrow range particle size 35±5.1 and high stability. HR-TEM, EDX results, Raman scattering, and XRD diffraction peaks all demonstrate the formation of high-quality ZnO NPs free of impurities and other secondary phases. Antibacterial activity assay of ZnO shows concentration dependent results with a good value of inhibition zone findings (18 mm for *E.coli* and 17.2 mm for *S.aureus*). The ZnO NPs synthesis by PLAW have a very good value of antibacterial assay results against the most popular pathogen (*E. coli* and *S. aureus*) which make it possible to be utilized in wound healing field.

Author contributions Author contributionsA.JH, SFK and SAM have formal analysis and prepared original draft.A.JH, SAM and MKS. investigation and data curation. SFK. and MKS.; validation. AJH. and SAM; supervision, project administration and approval of the final version of the draft.

Funding The authors have not disclosed any funding.

Declarations

Conflict of interest The authors declare no Conflict of interest.

References

Abbas, S.F., Haider, A.J., Al-Musawi, S.: Antimicrobial and wound healing effects of metal oxide nanoparticles-enriched wound dressing. Nano (2023). https://doi.org/10.1142/S1793292023300050

Abdulwahid, F.S., Haider, A.J., Al-Musawi, S.: Folate decorated dextran-coated magnetic nanoparticles for targeted delivery of ellipticine in cervical cancer cells. Adv. Nat. Sci.: Nanosci. Nanotechnol. **14**(1), 015001 (2023b)

Abdulwahid, F.S., Haider, A.J. and Al-Musawi, S.: Effect of laser parameter on Fe3O4 NPs formation by pulsed laser ablation in liquid. In: AIP Conference Proceedings, vol. 2769(1) (2023)

Abebe, B., Zereffa, E.A., AschalewTadesse, H.C., Murthy, A.: A review on enhancing the antibacterial activity of ZnO: mechanisms and microscopic investigation. Nanoscale Res. Lett. **15**(1), 1–19 (2020)

Ahmed, A.S., Salih, H.A., Hassoon, K.I., Kaur, S.: Stimulated Raman scattering of Q-Gaussian laser beam in an unmagnetized plasma. J. Appl. Sci. Nanotechnol. **3**(4), 10–19 (2023). https://doi.org/10.53293/jasn.2023.7035.1230

Al-Kinani, M.A., Haider, A.J., Al-Musawi, S.J.P.: Design and synthesis of nanoencapsulation with a new formulation of Fe@ Au-CS-CU-FA NPs by pulsed laser ablation in liquid (PLAL) method in breast cancer therapy: in vitro and in vivo. Plasmonics **16**(4), 1107–1117 (2021)

Almaary, K.S., Yassin, M.T., Elgorban, A.M., Al-Otibi, F.O., Al-Askar, A.A., Maniah, K.: Synergistic antibacterial proficiency of green bioformulated zinc oxide nanoparticles with potential fosfomycin synergism against nosocomial bacterial pathogens. Microorganisms **11**(3), 645 (2023)

Al-Obaidy, R., Haider, A.J., Al-Musawi, S., Arsad, N.J.S.R.: Targeted delivery of paclitaxel drug using polymer-coated magnetic nanoparticles for fibrosarcoma therapy: in vitro and in vivo studies. Sci. Rep. **13**(1), 3180 (2023)

Anu, N.T., Kumar, K., Sharma, K.K.: Application of Co-doped copper oxide nanoparticles against different multidrug resistance bacteria. Inorg. Nano-Met. Chem. **50**(10), 933–943 (2020). https://doi.org/10.1080/24701556.2020.1728554

Anwar, M.A., et al.: Antimicrobial resistance modulation of MDR *E. col*i by antibiotic coated ZnO nanoparticles. Microb. Pathog **148**, 104450 (2020)

Ashe, B.: A detail investigation to observe the effect of zinc oxide and Silver nanoparticles in biological system. M.Sc., National Institute of Technology, (Roll NO-607bm004) (2011)

Ashwini, J., Aswathy, T.R., Rahul, A.B., Thara, G.M., Nair, A.S.: Synthesis and characterization of zinc oxide nanoparticles using Acacia caesia bark extract and its photocatalytic and antimicrobial activities. Catalysts **11**(12), 1507 (2021)

Atrazina, K.M.T., Ruslimie, C., Razali, H., Khairul, W.: Catalytic study on TiO_2 photocatalyst synthesised via microemulsion method on atrazine. Sains Malays. **40**(8), 897–902 (2011)

Azam, A., Ahmed, A.S., Oves, M., Khan, M.S., Habib, S.S., Memic, A.: Antimicrobial activity of metal oxide nanoparticles against gram-positive and gram-negative bacteria: a comparative study. Int. J. Nanomed.Nanomed. **7**, 6003–6009 (2012)

Balkrishna, A., et al.: Phytoantioxidant functionalized nanoparticles: a green approach to combat nanoparticle-induced oxidative stress. Oxid. Med. Cell. Longev.. Med. Cell Longev. **2021**, 1–20 (2021)

Basosila, N., Inkoto, C., Maganga, O., Mbembo, B., Kasiama, G., Kabengele, C., Falanga, C., Masengo, C., Mpiana, P., Ngbolua, K.T.N.: Biogenic synthesis, spectroscopic characterization and bioactivity of *Cymbopogoncitratus* derived silver nanoparticles. J Appl Sci Nanotechnol **3**(4), 33–41 (2023). https://doi.org/10.53293/jasn.2023.7012.1226

Batros, S.S., Ali, M.H., Addie, A.J.: Microstructure-modulated antibacterial performance of chemically precipitated SnO2 nanoparticles. J. Appl. Sci. Nanotechnol. **3**(4), 20–32 (2023). https://doi.org/10.53293/jasn.2023.7107.1246

Bhosale, A., Abitkar, K., Sadalage, P., Pawar, K., Garadkar, K.: Photocatalytic and antibacterial activities of ZnO nanoparticles synthesized by chemical method. J. Mater. Sci. Mater. Electron. **32**, 20510–20524 (2021)

Cruz, D.M., et al.: Green nanotechnology-based zinc oxide (ZnO) nanomaterials for biomedical applications: a review. J. Phys.: Mater. **3**(3), 034005 (2020)

Cuscó, R., et al.: Temperature dependence of Raman scattering in ZnO. Phys. Rev. B **75**(16), 165202 (2007)

Danaei, M., et al.: Impact of particle size and polydispersity index on the clinical applications of lipidic nanocarrier systems. Pharmaceutics **10**(2), 57 (2018)

Dash, D., Panda, N., Sahu, D.J.A.S.S.: Photoluminescence and photocatalytic properties of europium doped ZnO nanoparticles. Appl. Surf. Sci. **494**, 666–674 (2019)

Debanath, M., Karmakar, S.J.M.L.: Study of blueshift of optical band gap in zinc oxide (ZnO) nanoparticles prepared by low-temperature wet chemical method. Mater. Lett. **111**, 116–119 (2013)

Drmosh, Q., Gondal, M., Yamani, Z., Saleh, T.J.A.S.S.: Spectroscopic characterization approach to study surfactants effect on ZnO2 nanoparticles synthesis by laser ablation process. Appl. Surf. Sci. **256**(14), 4661–4666 (2010)

Ehsan, S., Sajjad, M.: Bioinspired synthesis of zinc oxide nanoparticle and its combined efficacy with different antibiotics against multidrug resistant bacteria. J. Biomater. Nanobiotechnol. **08**(02), 159–175 (2017)

El-Gammal, R.E.J.I.J.C.R.: Antioxidative activity of nanoparticles of rosemary. J. Chemtech. Res. **9**, 844–854 (2016)

Flemban, T.H.: Synthesis, characterization, and analysis of zinc oxide nanoparticles using varying pulsed laser ablation energies in liquid. J. Exp. Nanosci. **18**(1), 2175817 (2023)

Fouda, A., et al.: The antimicrobial and mosquitocidal activity of green magnesium oxide nanoparticles synthesized by an aqueous peel extract of *Punicagranatum*. Chemistry **5**(3), 2009–2024 (2023)

George, S., et al.: Use of a rapid cytotoxicity screening approach to engineer a safer zinc oxide nanoparticle through iron doping. ACS Nano **4**(1), 15–29 (2010)

Goh, E., Xu, X., McCormick, P.J.S.M.: Effect of particle size on the UV absorbance of zinc oxide nanoparticles. Scripta Mater. **78**, 49–52 (2014)

Govindasamy, G.A., Mydin, R.B.S.M.N., Gadaime, N.K.R., Sreekantan, S.: Phytochemicals, biodegradation, cytocompatibility and wound healing profiles of chitosan film embedded green synthesized antibacterial ZnO/CuO nanocomposite. J. Polym. Environ.Polym. Environ. **89**, 1–17 (2023a)

Govindasamy, G.A., Mydin, R.B.S.M.N., Harun, N.H., Effendy, W.N.F.W.E., Sreekantan, S.: Giant milkweed plant-based copper oxide nanoparticles for wound dressing application: physicochemical, bactericidal and cytocompatibility profiles. Chem. Pap. **77**(2), 1181–1200 (2023b)

Haider, A.J., Sultan, F.I., Haider, M.J., Hadi, N.M.: Spectroscopic and structural properties of zinc oxide nanosphere as random laser medium. Appl. Phys. A **125**(4), 260 (2019)

Haider, A.J., Al-Kinani, M.A., Al-Musawi, S.J.K.E.M.: Preparation and characterization of gold coated super paramagnetic iron nanoparticle using pulsed laser ablation in liquid method. Key Eng. Mater. **886**, 77–85 (2021a)

Haider, A.J., Jabbar, A.A., Ali, G.A.: A review of pure and doped ZnO nanostructure production and its optical properties using pulsed laser deposition technique. J. Phys. Conf. Ser. **1795**(1), 012015 (2021b)

Haider, A.J., Alawsi, T., Haider, M.J., Taha, B.A., Marhoon, H.A.: A comprehensive review on pulsed laser deposition technique to effective nanostructure production: trends and challenges. Opt. Quant. Electron. **54**(8), 488 (2022)

Haider, A.J., et al.: Characterization of laser dye concentrations in ZnO nanostructures for optimization of random laser emission performance. Int. J. Modern Phys. B **38**(08), 2450111 (2023)

Haider, A.J., Sultan, F.I. and Al-Nafiey, A.: Controlled growth of different shapes for ZnO by hydrothermal technique. In: AIP Conference Proceedings, vol. 1968, no. 1 (2018)

He, G., Pearce, E.I.F., Sissons, C.H.: Inhibitory effect of ZnCl2 on glycolysis in human oral microbes. Arch. Oral Biol. **47**(2), 117–129 (2002)

Ishikawa, Y., Shimizu, Y., Sasaki, T., Koshizaki, N.: Preparation of zinc oxide nanorods using pulsed laser ablation in water media at high temperature. J. Coll. Interface Sci. **300**(2), 612–615 (2006)

Ismail, R.A., Sulaiman, G.M., Mohsin, M.H., Saadoon, A.H.: Preparation of silver iodide nanoparticles using laser ablation in liquid for antibacterial applications. IET Nanobiotechnol.Nanobiotechnol. **12**(6), 781–786 (2018)

Junlabhut, P., Mekprasart, W., Noonuruk, R., Chongsri, K., Pecharapa, W.: Characterization of ZnO: Sn nanopowders synthesized by co-precipitation method. Energy Procedia **56**, 560–565 (2014)

Jurablu, S., Farahmandjou, M., Firoozabadi, T.P.: Sol-gel synthesis of zinc oxide (ZnO) nanoparticles: study of structural and optical properties. J. Sci. **26**(3), 281–285 (2015)

Khan, A.: Raman spectroscopic study of the ZnO nanostructures. Pak. Mater. Soc. **4**(1), 5–9 (2010)

Khan, M.F., et al.: Flower-shaped ZnO nanoparticles synthesized by a novel approach at near-room temperatures with antibacterial and antifungal properties. Int. J. Nanomed.Nanomed. **9**, 853–864 (2014)

Khan, M.F., Ansari, A.H., Hameedullah, M., Ahmad, E., Husain, F.M., Zia, Q., Baig, U., Zaheer, M.R., Alam, M.M., Khan, A.M., AlOthman, Z.A., Ahmad, I., Ashraf, G., Aliev, G.: Sol-gel synthesis of thorn-like ZnO nanoparticles endorsing mechanical stirring effect and their antimicrobial activities: potential role as nano-antibiotics. Sci. Rep. **6**(1), 27689 (2016). https://doi.org/10.1038/srep27689

Khashan, K.S., Abbas, S.F.: Characterization of InN nanoparticles prepared by laser as photodetector. Int. J. Modern Phys. B **30**(14), 1650080 (2016)

Khashan, K.S., Abbas, S.F.J.I.J.N.: Indium nitride nanoparticles prepared by laser ablation in liquid. Int. J. Nanosci.Nanosci. **18**(02), 1850021 (2019)

Ko, T., et al.: ZnO nanopowders fabricated by dc thermal plasma synthesis. Mater. Sci. **134**(1), 54–58 (2006)

Kumar, R., Kumar, K., Sharma, S., Thakur, N., Thakur, N.: Multifunctional properties of microwave assisted CuO/Cu2O-ZnO mixed metal oxide nanocomposites. J. Mater. Sci. Mater. Electron. **34**(16), 1255 (2023a)

Kumar, P., Kumar, S., Thakur, N.: Azadirachta indica and polyvinylpyrrolidone encapsulated Fe_2O_3 nanoparticles to enhance the photocatalytic and antioxidant activity. Inorg. Chem. Commun. **155**, 111084 (2023b)

Madathil, A.N.P., Vanaja, K.A. and Jayaraj, M.: Synthesis of ZnO nanoparticles by hydrothermal method. In: Nanophotonic materials IV, vol. 6639, pp. 47–55 (2007)

Maqbool, Q., et al.: Antimicrobial potential of green synthesized CeO2 nanoparticles from *Olea europaea* leaf extract. Int. J. Nanomed.Nanomed. **11**, 5015–5025 (2016)

Pal, S., Tak, Y.K., Song, J.M.: Does the antibacterial activity of silver nanoparticles depend on the shape of the nanoparticle? A study of the gram-negative bacterium *Escherichia coli*. Appl. Environ. Microbiol. Environ Microbiol **73**(6), 1712–1720 (2007)

Premanathan, M., Karthikeyan, K., Jeyasubramanian, K., Manivannan, G.J.N.N.: Biology, and Medicine, Selective toxicity of ZnO nanoparticles toward gram-positive bacteria and cancer cells by apoptosis through lipid peroxidation. Nanomed. Nanotechnol. Biol. Med.: Nanotechnol Biol Med **7**(2), 184–192 (2011)

Rashid, S.N., Aadim, K.A., Jasim, A.S., Hamad, A.M.: Synthesized zinc nanoparticles via pulsed laser ablation: characterization and antibacterial activity. Karbala Int. J. Modern Sci. **8**(3), 462–476 (2022)

SagarRaut, D.P., Thorat, R.: Green synthesis of zinc oxide (ZnO) nanoparticles using *OcimumTenuiflorum* leaves. Int. J. Sci. Res. **4**, 1225–1228 (2015)

Sahoo, S.: Socio-ethical issues and nanotechnology development: Perspectives from India. In: 10th IEEE International Conference on Nanotechnology, pp. 1205–1210 (2010)

Salman, J.A.S., Kadhim, A.A., Haider, A.J.: Biosynthesis, characterization and antibacterial effect of ZnO nanoparticles synthesized by *Lactobacillus* Spp. Global Pharma Technol **10**(03), 348–355 (2018)
Šćepanović, M., Grujić-Brojčin, M., Vojisavljević, K., Bernik, S., Srećković, T.: Raman study of structural disorder in ZnO nanopowders. J. Raman Spectrosc. **41**(9), 914–921 (2010)
Shinde, S.S.: Antimicrobial activity of ZnO nanoparticles against pathogenic bacteria and fungi. Sci Med Central **3**, 1033 (2015)
Sirelkhatim, A., et al.: Review on zinc oxide nanoparticles: antibacterial activity and toxicity mechanism. Nano-Micro Lett. **7**, 219–242 (2015)
Solati, E., Mashayekh, M., Dorranian, D.J.A.P.A.: Effects of laser pulse wavelength and laser fluence on the characteristics of silver nanoparticle generated by laser ablation. Appl. Phys. A **112**, 689–694 (2013)
Solati, E., Dejam, L., Dorranian, D.J.O., Technology, L.: Effect of laser pulse energy and wavelength on the structure, morphology and optical properties of ZnO nanoparticles. Opt. Laser Technol. **58**, 26–32 (2014)
Sukhdev, A., Challa, M., Narayani, L., Manjunatha, A.S., Deepthi, P.R., Angadi, J.V., Mohan Kumar, P., Pasha, M.: Synthesis, phase transformation, and morphology of hausmannite Mn3O4 nanoparticles: photocatalytic and antibacterial investigations. Heliyon **6**(1), e03245 (2020). https://doi.org/10.1016/j.heliyon.2020.e03245
Talam, S., Karumuri, S.R., Gunnam, N.: Synthesis, characterization, and spectroscopic properties of ZnO nanoparticles. ISRN Nanotechnol. **2012**, 1–6 (2012)
Tanna, J.A., Chaudhary, R.G., Juneja, H.D., Gandhare, N.V., Rai, A.R.J.B.: Histidine-capped ZnO nanoparticles: an efficient synthesis, spectral characterization and effective antibacterial activity. BioNanoScience **5**, 123–134 (2015)
Thakur, N., Kumar, K.: Effect of (Ag, Co) co-doping on the structural and antibacterial efficiency of CuO nanoparticles: a rapid microwave assisted method. J. Environ. Chem. Eng. **8**(4), 104011 (2020)
Thakur, N., Thakur, N.: Removal of organic dyes and free radical assay by encapsulating polyvinylpyrrolidone and *Tinospora Cordifolia* in dual (Co–Cu) doped TiO2 nanoparticles. Environ. Pollut. **335**, 122229 (2023)
Thakur, N., Kumar, K., Kumar, A.: Effect of (Ag, Zn) co-doping on structural, optical and bactericidal properties of CuO nanoparticles synthesized by a microwave-assisted method. Dalton Trans. **50**(18), 6188–6203 (2021)
Umar, K., et al.: ZnO Nano-swirlings for Azo dye AR183 photocatalytic degradation and antimycotic activity. Sci. Rep. **12**(1), 14023 (2022)
VeleshKolaei, M.R.H., Gill, P., Rafati, A., Adiani, M.: Bioinformatical prediction of G-quadruplex aptamer for detection of a ligand in practice. J. Appl. Sci. Nanotechnol. **3**(4), 1–9 (2023). https://doi.org/10.53293/jasn.2023.7058.1234
Wang, Y., et al.: Structure, luminescence and photocatalytic activity of Mg-doped ZnO nanoparticles prepared by auto combustion method. Mater. Sci. Semicond. Process. **29**, 372–379 (2015)
Xin-Hua, L., Jia-Yue, X., Min, J., Hui, S., Xiao-Min, L.J.C.P.L.: Electrical and optical properties of bulk ZnO single crystal grown by flux Bridgman method. Chin. Phys. Lett. **23**(12), 3356–3358 (2006)
Yousif, A.A., Habubi, N.F., Haidar, A.: Nanostructure zinc oxide with cobalt dopant by PLD for gas sensor applications. J. Nano- Electron. Phys. **4**(2), 02007–02011 (2012)
Yudasari, N., Wiguna, P.A., Suliyanti, M.M., Imawan, C.: Antibacterial activity of ZnO nanoparticles fabricated using laser ablation in solution technique. J. Phys. Conf. Ser. **1245**(1), 012035 (2019)
Zare, M., Namratha, K., Byrappa, K., Surendra, D., Yallappa, S., Hungund, B.: Surfactant assisted solvothermal synthesis of ZnO nanoparticles and study of their antimicrobial and antioxidant properties. J. Mater. Sci. Technol. **34**(6), 1035–1043 (2018)
Zhou, W., Tang, D., Liu, R., Zou, B.: Structure and optical properties of pure and doped ZnO 1D nanostructures. Mater. Lett. **91**, 369–371 (2013)
Zhu, P., et al.: Biomedical applications of functionalized ZnO nanomaterials: from biosensors to bioimaging. Adv. Mater. Interfaces **3**(1), 1500494 (2016)